Thermal evolution of silicon carbide electronic bands

E. Cannuccia[1,2] and A. Gali[3,4]

[1]*Aix-Marseille Université, Laboratoire de Physique des Interactions Ioniques et Moléculaires (PIIM), UMR CNRS 7345, F-13397 Marseille, France*

[2]*Dipartimento di Fisica, Università di Roma, Tor Vergata, Via della Ricerca Scientifica 1, I–00133 Roma, Italy*

[3]*Wigner Research Centre for Physics, P.O. Box 49, H-1525, Budapest, Hungary*

[4]*Department of Atomic Physics, Budapest University of Technology and Economics, Budafoki út 8., H-1111 Budapest, Hungary*

(Received 11 July 2019; published 2 January 2020)

Direct observation of temperature dependence of individual bands of semiconductors for a wide temperature region is not straightforward, in particular. However, this fundamental property is a prerequisite in understanding the electron-phonon coupling of semiconductors. Here we apply *ab initio* many-body perturbation theory to the electron-phonon coupling on hexagonal silicon carbide (SiC) crystals and determine the temperature dependence of the bands. We find a significant electron-phonon renormalization of the band gap at 0 K. Both the conduction and valence bands shift at elevated temperatures, exhibiting a different behavior. We compare our theoretical results with the observed thermal evolution of SiC band edges, and discuss our findings in the light of high-temperature SiC electronics and defect qubits operation.

DOI: 10.1103/PhysRevMaterials.4.014601

I. INTRODUCTION

Electron-phonon interaction impacts a large variety of fundamental materials properties [1], from the critical temperature of superconductors to the zero-point renormalization and the temperature dependence of the electronic energy bands, from the electronic band gaps [2–6] to the thermal evolution of the optical spectra and excitonic lifetimes [7–9]. In addition, the electron-phonon coupling contributes to the optical absorption and emission in indirect gap semiconductors [10–12], determines the electronic carrier mobility of semiconductors [13], the carrier relaxation rates [14], the distortion of band structures, and phonon dispersion, giving rise to kinks and Kohn anomalies in photoemission [15].

The thermal evolution of the band structure and band gap arises from the thermal expansion effect and from the coupling of electrons with phonons, leading to a renormalization of the electronic states. The latter effect is in most of the cases the dominant one, being larger than the thermal expansion [2]. The strength of renormalization depends on temperature, so valence and conduction bands may be shifted differently, leading usually to a shrinking of the gap [2], although an anomalous behavior (i.e., gap increases with temperature) is found in other cases [16].

Direct observation of the temperature evolution of individual bands over a wide region of temperatures is not straightforward. Optical techniques are capable of measuring band gaps, and not the absolute values of the valence band maximum (VBM) and the conduction band minimum (CBM) separately. The interpretation of results from optical techniques is then weakly conclusive. In addition, the indirect band-gap nature of some materials prohibits the direct optical transition between VBM and CBM, which turns out to be allowed only when phonons assist the optical excitation. Recent attempts used Si $2p$ core level as a reference to extract the CBM and VBM energy position of Si and hexagonal 6H silicon carbide (SiC) crystals [see Fig. 1(a)] from the onset of soft x-ray absorption spectroscopy (XAS) and soft non-resonant x-ray emission spectroscopy (XES), respectively [17,18]. This method assumes temperature-independent core exciton binding energy [19], which results in a systematically smaller derived band gap than the observed optical band gap, and it may suffer from the accurate observation of the onset energies at elevated temperatures caused by temperature broadening effects. We stress that none of these methods enables the observation of individual bands other than band edges but observation of the temperature dependence of those bands can be an important issue at high temperatures. It is utterly important to apply *ab initio* many-body perturbation theory that can provide valuable insights on the electron-phonon coupling effect in semiconductors by directly describing the temperature dependence of individual bands. This fundamental property has been recently studied, typically only for the band edges and up to room temperature [4,5,7]. Here we are interested to extend these investigations to higher temperatures for hexagonal 4H and 6H SiC crystals [see Fig. 1(a)] and, in particular, we aim to get the temperature dependence of the first and second conduction bands to establish the effect of the latter on the conductivity. The choice of these materials was motivated by three points: (i) experimental data are available for the temperature dependence of 4H SiC gap [20] as well as 4H SiC-based semiconductor devices, which have been successfully tested at high temperatures (around 800 K) for Venus mission [21], where deep insight into the electron-phonon interaction of electronic bands has an uttermost importance; (ii) since both experimental data for temperature-dependence gap [22] and band edges [18] of 6H SiC are available, this compound is eligible for validation of the theoretical methods which rely on the electron-phonon renormalization of electronic states; and (iii) SiC is a semiconductor platform for hosting hybrid

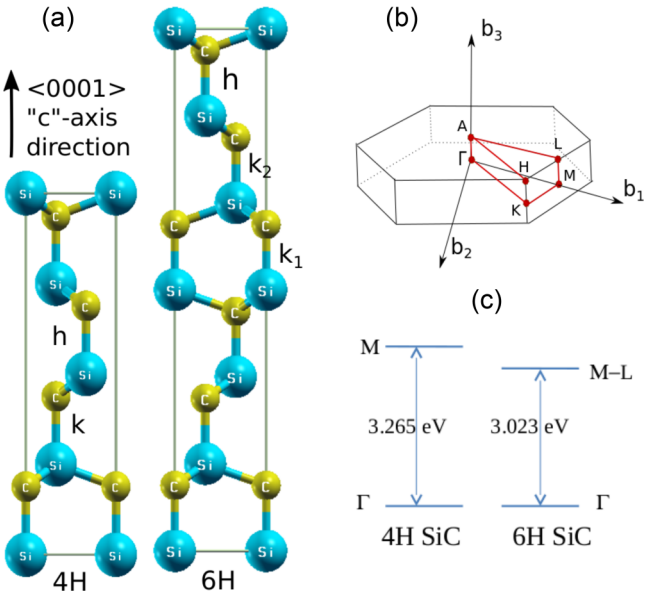

FIG. 1. (a) Primitive cells of 4*H* and 6*H* SiC with *k* (k_1, k_2) and *h* Si-C bilayers, where *k* and *h* refer to quasicubic and hexagonal sites. (b) Brillouin zone of hexagonal SiC polytypes. (c) Sketch of band gap of hexagonal SiC crystals. In 4*H* SiC, the first (M_1) and second (M_2) conduction bands are close in energy [37]. In 6*H* SiC, the lowest conduction band is very flat along the $M - L$ line [38,39], and it should be close to the *M* point [c].

opto-electro-mechanical defect quantum bits [23–33]. These defect quantum bits require very accurate electrical and optical control which depend on the ionization thresholds, i.e., the position of band edges at the operation temperature [34–36].

II. COMPUTATIONAL METHODS

We perform geometry optimization, electronic structure and phonons calculation, followed by the calculation of electron-phonon matrix elements, and renormalization of the electronic energies as a function of temperature [see Supplemental Material (SM) Ref. [40] for further details]. Density-functional theory (DFT) and density-functional perturbation theory (DFPT) calculations are carried out using QUANTUM ESPRESSO 6.1.0 suite [41]. We employ norm-conserving pseudopotentials and the exchange-correlation functional is described by the local density approximation (LDA) with the Perdew-Zunger parametrization [42]. We perform, in a first step, a full optimization (starting from experimental lattice parameters and atomic positions along $\vec{c}$ axis [38,43]) using 90 Ry as kinetic energy cutoff, $18 \times 18 \times 6$ and $18 \times 18 \times 4$ *k* meshes of the Brillouin-zone (BZ) for 4*H* and 6*H* SiC crystals, respectively. The phonon frequencies are obtained with the same kinetic energy cutoff on $10 \times 10 \times 3$ and $10 \times 10 \times 2$ q meshes, respectively, and then interpolated along the q path connecting $\Gamma - K - M - \Gamma$ high symmetry points of hexagonal systems Brillouin zone [see Fig. 1(b) and SM for symmetry analysis of phonon modes, phonon dispersion curves, and comparison between theoretical and experimental phonon frequencies at Γ point for 4*H* and 6*H* SiC [44–49]].

The same *k*-point sampling of the Brillouin zone and cutoff are used to calculate the derivatives of the self-consistent Kohn-Sham potential with respect to the atomic positions needed to evaluate the electron-phonon coupling matrix elements. A denser q grid ($12 \times 12 \times 3$ and $12 \times 12 \times 3$ q meshes for 4*H* and 6*H* SiC, respectively) results in a difference of less than 10%, thus we estimate it as an upper bound of our accuracy. Unoccupied bands as many as five times the number of the occupied ones are taken into account for 4*H* SiC. On the other hand, for 6*H* we are bound to use 96 unoccupied bands (four times the number of occupied ones) because of technicalities in the applied algorithms and computational capacity. We note that this affects the convergence of 6*H* SiC results as discussed in the SM. We will present the extrapolated convergent values for 6*H* SiC that are estimated from the convergence study of 4*H* SiC results.

III. THEORETICAL BACKGROUND

The key issue of this study is the calculation of the temperature-dependent correction to the electronic state $|n\mathbf{k}\rangle$, with energy $\varepsilon_{n\mathbf{k}}$ due to the electron-phonon interaction. The electron-phonon interaction is treated perturbatively [50,51]

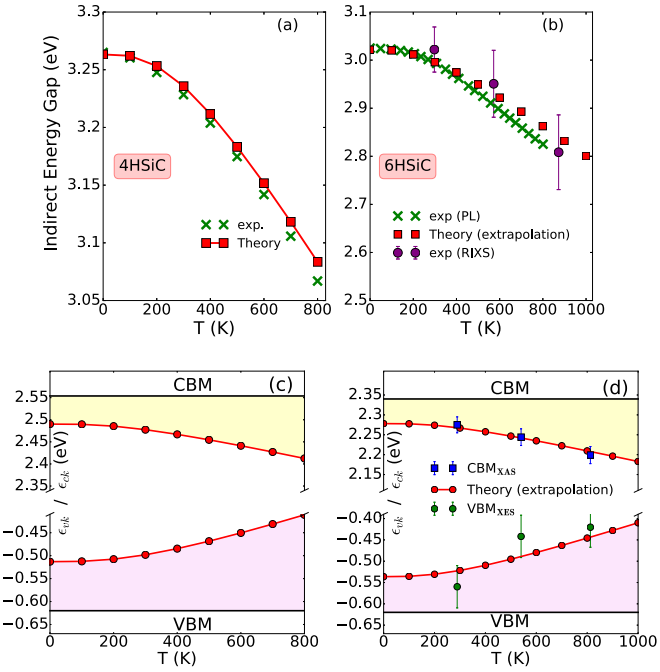

FIG. 2. Calculated thermal evolution of indirect band gaps in the temperature range $0 - 800$ K for 4*H* SiC (a) and $0 - 1000$ K for 6*H* SiC (b). The calculated curves are aligned to the experimental data at $T = 0$ K after having applied the GW correction to the indirect gap. For 6*H*, an extrapolation at 150 bands (red squares: estimated convergent data) is given for comparison. The experimental data [green crosses in (a) and (b)] of the optical gaps are taken from Refs. [22,61]. The others (violet dots) have been extracted from RIXS spectra (Ref. [18]), with correction of the core-hole exciton binding energy included. Thermal evolution of calculated VBM and CBM of (c) 4*H* SiC and (d) 6*H* SiC, where the latter is compared to the XAS and XES measurements (Ref. [18]) rescaled to 99.5 eV and 98.65 eV, respectively, to match the temperature evolution of CBM and VBM. Notice that on top of the electron-phonon correction the quasiparticle correction has been also added.

within Heine Allen Cardona (HAC) approach [52–54] as implemented in YAMBO [55] code, by considering the first- and second-order Taylor expansion of the self-consistent potential $V_{\rm scf}(\mathbf{r})$ [56] in the nuclear displacements $\mathbf{u}_{Is}$ with respect to the equilibrium positions $\mathbf{R}_{Is} = \mathbf{R}_I + \tau_s$ for the atom s inside cell I (the cell is located at position R_I) at the position τ_s. Standard perturbation theory is then applied. The first-order Taylor expansion of $V_{\rm scf}(\mathbf{r})$ is treated within the second–order perturbation theory, while the second-order Taylor expansion is treated within the first-order perturbation theory. The corresponding temperature-dependent energy shift of the electronic state is then composed of Fan and Debye-Waller (DW) contributions.

The Fan term is given by

$$\Delta\varepsilon^{\rm Fan}_{n\mathbf{k}}(T) = \sum_{\mathbf{q}\lambda}\frac{1}{N}\sum_{n'}\frac{\left|g^{\mathbf{q}\lambda}_{n'n\mathbf{k}}\right|^2}{\varepsilon_{n\mathbf{k}} - \varepsilon_{n'\mathbf{k}+\mathbf{q}}} \times (2B(\omega_{\mathbf{q}\lambda}) + 1), \quad (1)$$

where $\omega_{\mathbf{q}\lambda}$ are the phonon frequencies calculated *ab initio* using DFPT, while $B(\omega_{\mathbf{q}\lambda})$ is the Bose function distribution, $\varepsilon_{n\mathbf{k}}$ are the DFT bare electronic energies, N is the number of $\mathbf{q}$ points, and $\left|g^{\mathbf{q}\lambda}_{n'n\mathbf{k}}\right|^2$ are the electron-phonon matrix elements for the scattering between the electronic states $|n\mathbf{k}\rangle$ and $|n'\mathbf{k} + \mathbf{q}\rangle$ via the phonon $\mathbf{q}\lambda$, defined as

$$g^{\mathbf{q}\lambda}_{n'n\mathbf{k}} = \sum_{s\alpha}(2M_s\omega_{\mathbf{q}\lambda})^{-1/2}e^{i\mathbf{q}\cdot\tau_s} \times \langle n'\mathbf{k}+\mathbf{q}|\frac{\partial V_{\rm scf}(\mathbf{r})}{\partial R_{s\alpha}}|n\mathbf{k}\rangle\xi_\alpha(\mathbf{q}\lambda|s), \quad (2)$$

where M_s is the atomic mass, τ_s is the position of the atomic displacement in the unit cell, and $\xi_\alpha(\mathbf{q}\lambda)$ are the Cartesian components α of the phonon polarization vectors corresponding to the phonon momentum $\mathbf{q}$ and branch λ. We have also used the short form $R_{s\alpha} = R_{Is\alpha}|_{I=0}$.

The DW contribution reads as

$$\Delta\varepsilon^{\rm DW}_{n\mathbf{k}}(T) = -\frac{1}{2}\sum_{\mathbf{q}\lambda}\frac{1}{N}\sum_{n'}\frac{\Lambda^{\mathbf{q}\lambda}_{nn'\mathbf{k}}}{\varepsilon_{n\mathbf{k}} - \varepsilon_{n'\mathbf{k}}} \times [2B(\omega_{\mathbf{q}\lambda}) + 1], \quad (3)$$

where $\Lambda^{\mathbf{q}\lambda}_{nn'\mathbf{k}}$ is an expression written in terms of $\nabla V_{\rm scf}$ and obtained by imposing the translation invariance of $\Delta\varepsilon_{n\mathbf{k}}$ when all atoms in the crystal are displaced the same amount from their equilibrium positions [52]. It is worth noticing that from Eqs. (1) and (3) when the temperature (T) vanishes, the energy correction does not vanish due to the $[2B(\omega_{\mathbf{q}\lambda}) + 1]$ factor yielding the zero-point motion renormalization (ZPMR).

IV. RESULTS AND DISCUSSION

Since the thermal expansion minutely increases the lattice constants of hexagonal SiC [59], the thermal evolution of the band structure and of the electronic gap will be caused mainly by the electron-phonon interaction. We assess first the HAC approach to describe the thermal evolution of 4*H* and 6*H* SiC indirect band gaps [see Fig. 1(c) for a sketch of indirect band gaps in both samples]. At $T = 0$ K, we found 0.17 eV and 0.14 eV for 4*H* and 6*H* SiC, respectively, as of the indirect electronic band gaps. These values are about 5% of the indirect electronic band gaps, revealing an intermediate ZPMR value in between bulk silicon and diamond [3,60]. The calculated temperature dependence of the indirect band gap can be compared to that of the observed optical gap of SiC crystals [22,61]. In Figs. 2(a) and 2(b), the calculated temperature-dependent indirect band gaps are aligned to the experimental data at $T = 0$ K after having applied the electron quasiparticle (QP) correction as a simple scissor on the DFT-LDA band gaps. The temperature evolution agrees very well with the experimental data as derived from the optical gaps for a wide range of temperatures, which allows us to predict a shrinking of the electronic gap of about 0.35 eV (4*H* SiC) and 0.30 eV (6*H* SiC) at $T = 800$ K. The shrinkings of the electronic gap of 6*H* SiC have been estimated as we will explain later and in the SM in detail.

The above briefly mentioned opening of the indirect gap due to QP effects has been calculated adopting the Godby-Needs plasmon-pole model of the so-called GW method, where the self-energy Σ is expanded in terms of the single particle Green's function G and the screened Coulomb interaction W [62–65]. This method yields a 0.92 eV QP-level correction for both 4*H* and 6*H* SiC. We used $18 \times 18 \times 6$ and $16 \times 16 \times 3$ k-point sets for 4*H* and 6*H* SiC, respectively, with 200 bands in the numerically convergent GW [63,64] calculations. Our correction results are lower with respect to those calculated by Ummels *et al.* [58] [see Table I]. This is due to the different plasmon pole model used (see Refs. [66–68] and SM for a further discussion on previous QP calculations on these systems). Our LDA energies for the highest valence band and the lowest conduction bands at Γ and M points, in agreement with literature [38,69,70], are listed in Table I together with previous GW gaps [58] and experimental data [20]. The experimental data comes from optical measurements in which the exciton binding energies should be accounted for comparison to the calculated electronic band gaps. These binding energies are experimentally found to be 0.020 eV and 0.078 eV in 4*H* and 6*H* SiC [71,72], respectively, i.e., which are smaller than the expected accuracy of the GW calculations.

Next, we study the temperature dependence of the individual bands. In particular, we focus on the VBM and CBM [see Figs. 2(c) and 2(d)], whose difference provides the indirect band gap plotted in Figs. 2(a) and 2(b), once it is opportunely rescaled to match the experimental data at $T = 0$ K. Here we applied the contribution of each band to the GW QP correction, −0.62 eV for the VBM and +0.30 eV for the CBM for both systems. Since VBM and CBM do not occur at the same point of the BZ, they have different symmetries and they interact differently with phonons. For 4*H* and 6*H* SiC, in fact, we predict an asymmetry in the band gap closing, where the contribution from the VBM is larger, respectively ∼63% and ∼58% of the total band gap shrinking. Here, we stress that the latter result has been estimated. We used the converged data set for 4*H* SiC (see Fig. S3 of SM) to extrapolate convergent data for 6*H* SiC because an explicit convergent calculation is computationally prohibitive as explained in the SM. In Fig. 2(d), we report the temperature-dependent XAS and XES spectra which depict, respectively, the CBM and VBM behavior in 6*H* SiC [18]. Both XAS and XES experimental data

TABLE I. Energies of the lowest conduction band (first line) and the highest valence band (second line) at high symmetry points in the hexagonal BZ with different levels of theory compared to the experimental data. The energy bands are referred to the valence band maximum at Γ point, which is set to zero. For M point, we give the first and second lowest conduction band positions. In addition, the indirect band gap (E_g^{ind}) is reported together with the optical gaps. The quasiparticle-level correction for the direct gap at Γ is also given in the last column.

	Γ	M	DFT-LDA E_g^{ind}	GW E_g^{ind}		Optical gap[a]	GW corr. (dir)
Polytype	(eV)	(eV)	(eV)	this paper (eV)	other works[b] (eV)	(eV)	(eV)
4H	5.18	2.25 2.34	2.25	3.17	3.35	3.27	0.97
	0.00	−1.14					
6H	5.27	2.04 2.21	2.04	2.96	3.24	3.02	0.98
	0.00	−1.11					

[a]Refs. [22,57]
[b]Ref. [58]

have been shifted to match the temperature evolution of CBM and VBM. We find a very good agreement with XAS-derived data. The XES one also agrees with the estimated converged data set. Our theory well supports the observed temperature evolution of the indirect band gap of 4H SiC.

The nature of the electron-phonon-coupling-induced renormalization in 4H and 6H SiC can be analyzed in the light of plotted Eliashberg function (Fig. 3), where the separate contribution of Fan and DW terms is highlighted. For both 4H and 6H SiC, the VBM states are mostly coupled to the optical phonons (LO and TO) starting from 700 cm^{-1}. In this phonon frequency energy range, both Fan and DW have a significant weight in the energy renormalization while they almost cancel each other in the acoustic phonon frequency range. On the other hand, the CBM states (here called M_1) and the second lowest conduction band (here called M_2) also couple to acoustic phonons already from 220 cm^{-1}. Most of the contribution is given by the Fan term, which dominates all over the whole phonon frequency range. The difference between the CBM and VBM Eliashberg functions, being negative, is strictly related to the temperature dependence of the fundamental band gap shown in Fig. 2. The square modulus of VBM wave function shows that the charge density is mainly localized on the Si-C bond of the hexagonal Si-C layer (off-axis Si-C bonds). The coupling with planar optic modes, as highlighted by the Eliashberg functions, is then justified, as these vibrations change the length of the interatomic bonds in which the charge density associated with the VBM resides [60]. The CBM states are localized in the interstitial places of 4H and 6H SiC lattice [73], in contrast to the bond-localized charge density of the VBM. The coupling with optical modes slightly loses weight and is transferred to acoustic modes.

We observe now that the calculated lowest-energy conduction bands of 4H SiC labeled as M_1 and M_2 are quite close in energy [see Table I]. According to a recent measurement, the energy separation of the two lowest conduction bands at the M point of the Brillouin zone is 144 ± 2 meV at 2 K [37].

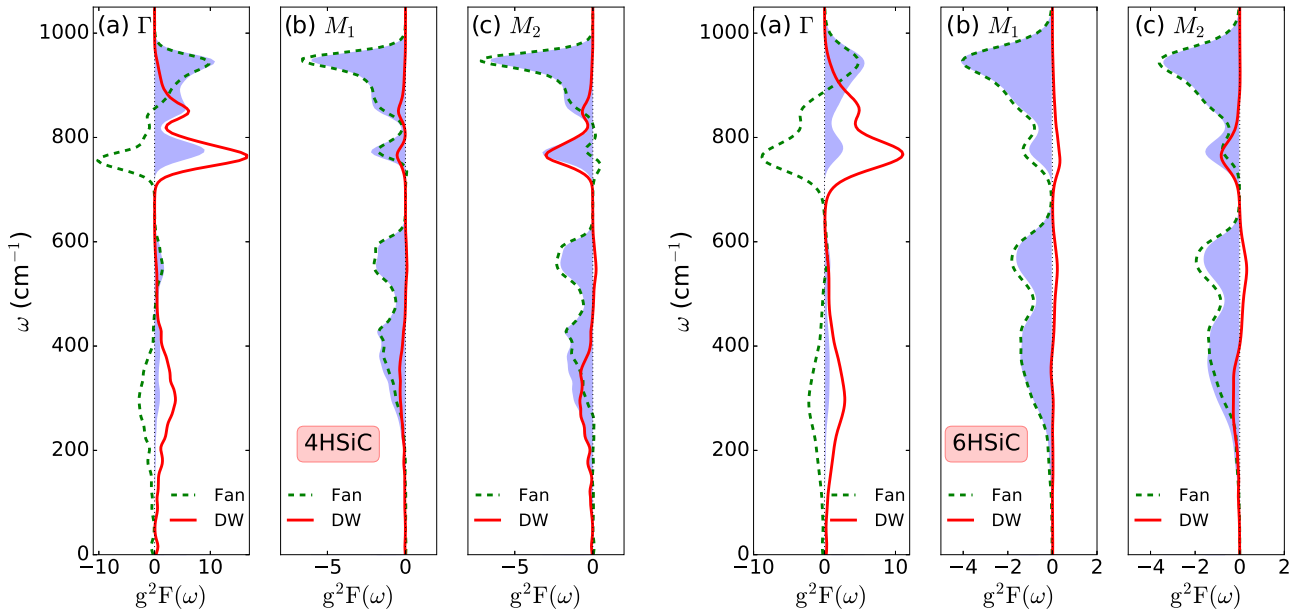

FIG. 3. Generalized electron-phonon Eliashberg function for 4H and 6H SiC (a) valence band maximum (Γ point), (b) first conduction band minimum (M_1 point), and (c) second conduction band minimum (M_2-point). Fan and Debye-Waller (DW) contributions are shown separately with dashed and solid lines, respectively. The blue shaded areas represent the total Eliashberg function.

If these two bands crossed at elevated temperatures, then this could seriously affect the n-type conductivity of the SiC-based electronic devices. We find that the energy separation between M_1 and M_2 only reduces by 5 meV (<5%), going from 0 K to 800 K temperatures [see Fig. S4 in the SM], because both M_1 and M_2 bands shift downward with increasing temperatures. We note that similar properties are found in 6H SiC [see Fig. S4 in SM]. The calculated effective masses of the M_1 and M_2 bands [see Table SII in the SM and Ref. [74]] imply that the conductivity of the M_2 band is smaller than that of the M_1 band except in the $K-M$ direction. However, the overall conductivity [75,76] still increases [see Fig. S5 in SM] because of a larger number of typical nitrogen donors ionization at k and h sites at 120 and 60 meV [77], respectively, with increasing temperatures. This paves the way for space agencies to employ 4H SiC-based integrated circuits to probe the surface of Venus, where the temperature is ≈730 K [21].

Our fundamental study has implications on the quantum bits hosted by 4H SiC such as neutral divacancies [24,25]. Divacancy qubits are initialized and read out by optically detected magnetic resonance [25], where illumination at about 1.17 eV used in this process may lead to a dark state, i.e., a permanent loss of qubits [34–36]. The qubit state can be restored by applying ∼1.3 eV optical excitation [34–36], where the nature of the dark state was debated in the literature [34,35,78]. According to one of the most recent studies [36], the dark state can be identified as the negative charge state of divacancies where optical excitation at ∼1.25 eV is the threshold of photoionization of the electron from the in-gap defect level to the conduction band edge at cryogenic temperatures. The coherent control of defect spins in 4H SiC can be achieved even at high temperatures up to 600 K [79], paving the way for SiC-based broad-temperature-range quantum sensing such as magnetic and temperature sensing. As the typical excitation energy of the qubit and the threshold for photoionization of the dark state are close in energy, the temperature-dependent band edge and photoionization energies can seriously affect the stability of the charge state of divacancies, i.e., the operation of divacancy qubits. We find that the CBM of 4H SiC shifts down by 0.1 eV, going from cryogenic temperatures up to 600 K. This implies that the threshold for photoionization reduces ∼0.1 eV. We conclude that high-temperature operation of 4H SiC divacancy qubits would be stable against photoionization.

V. SUMMARY AND CONCLUSION

In this study, we applied DFT on the electronic structure and phonons in 4H and 6H SiC, and determine the electron-phonon coupling within HAC approach [52–54]. We find a sizable temperature-dependent renormalization energy on the electronic structure for both crystals. As a consequence, both valence and conduction band edges shift with temperature, thus affecting the operation of defect qubits at elevated temperatures. We predict that the operation of divacancy qubits in 4H SiC [24,25] is stabilized at elevated temperatures against bleaching caused by photoionization. Furthermore, our *ab initio* results indicate that the two lowest conduction bands do not cross at elevated temperature and the conductivity of doped 4H SiC is not much affected, thus SiC electronics conforms to high temperature operation.

We conclude that SiC exhibits favorable properties for hosting electronic devices at extreme high-temperature operation, which is important for next-generation sensors and electronics in space missions. Our study has an impact on quantum technology applications too, and serves as a template for similar studies in other semiconductors.

ACKNOWLEDGMENTS

E.C. acknowledges support by the Programma per Giovani Ricercatori—2014 Rita Levi Montalcini, French HPC computational resources from GENCI-CCRT and TGCC, through Grant No. 2017-910165 and ISCRAC Italian Cineca Project No. HP10CEPHVH. The support from the EU Commission and the National Office of Research, Development, and Innovation in Hungary (NKFIH) in the QuantERA Nanospin project (NKFIH Grant No. 127902), the support from NKFIH in the National Quantum Technology Program (NKFIH Grant No. 2017-1.2.1-NKP-2017-00001), in the NVKP Program (NKFIH Grant No. NVKP_16-1-2016-0043) and the National Excellence Program (Grant No. KKP129866) is acknowledged. The support from the EU Commission in the H2020 project QuanTELCO (Grant No. 862721) is acknowledged.

[1] F. Giustino, Rev. Mod. Phys. **89**, 015003 (2017).
[2] M. Cardona and S. Gopalan, in *Progress in Electron Properties of Solids: Festschrift in Honour of Franco Bassani*, Physics and Chemistry of Materials with Low-Dimensional Structures, edited by E. Doni, R. Girlanda, G. P. Parravicini, and A. Quattropani (Springer, Netherlands, Dordrecht, 1989), pp. 51–64.
[3] M. Cardona and M. L. W. Thewalt, Rev. Mod. Phys. **77**, 1173 (2005).
[4] E. Cannuccia and A. Marini, Phys. Rev. Lett. **107**, 255501 (2011).
[5] E. Cannuccia and A. Marini, Eur. Phys. J. B **85**, 320 (2012).
[6] A. Gali, T. Demján, M. Vörös, G. Thiering, E. Cannuccia, and A. Marini, Nat. Commun. **7**, 11327 (2016).
[7] A. Marini, Phys. Rev. Lett. **101**, 106405 (2008).
[8] H. Kawai, K. Yamashita, E. Cannuccia, and A. Marini, Phys. Rev. B **89**, 085202 (2014).
[9] A. Molina-Sánchez, M. Palummo, A. Marini, and L. Wirtz, Phys. Rev. B **93**, 155435 (2016).
[10] J. Noffsinger, E. Kioupakis, C. G. Van de Walle, S. G. Louie, and M. L. Cohen, Phys. Rev. Lett. **108**, 167402 (2012).
[11] F. Paleari, H. P. C. Miranda, A. Molina-Sánchez, and L. Wirtz, Phys. Rev. Lett. **122**, 187401 (2019).
[12] E. Cannuccia, B. Monserrat, and C. Attaccalite, Phys. Rev. B **99**, 081109(R) (2019).
[13] S. Poncé, E. R. Margine, and F. Giustino, Phys. Rev. B **97**, 121201(R) (2018).

[14] A. Molina-Sánchez, D. Sangalli, L. Wirtz, and A. Marini, Nano Lett. **17**, 4549 (2017).

[15] F. Forster, A. Molina-Sánchez, S. Engels, A. Epping, K. Watanabe, T. Taniguchi, L. Wirtz, and C. Stampfer, Phys. Rev. B **88**, 085419 (2013).

[16] C. E. P. Villegas, A. R. Rocha, and A. Marini, Nano Lett. **16**, 5095 (2016).

[17] M. Beye, F. Hennies, M. Deppe, E. Suljoti, M. Nagasono, W. Wurth, and A. Föhlisch, New J. Phys. **12**, 043011 (2010).

[18] P. S. Miedema, M. Beye, R. Könnecke, G. Schiwietz, and A. Föhlisch, J. Electron Spectrosc. Relat. Phenom. **197**, 37 (2014).

[19] R. Buczko, G. Duscher, S. J. Pennycook, and S. T. Pantelides, Phys. Rev. Lett. **85**, 2168 (2000).

[20] W. J. Choyke, D. R. Hamilton, and L. Patrick, Phys. Rev. **133**, A1163 (1964).

[21] P. G. Neudeck, R. D. Meredith, L. Chen, D. J. Spry, L. M. Nakley, and G. W. Hunter, AIP Adv. **6**, 125119 (2016).

[22] W. J. Choyke, Mater. Res. Bull. **4**, S141 (1969).

[23] J. R. Weber, W. F. Koehl, J. B. Varley, A. Janotti, B. B. Buckley, C. G. Van de Walle, and D. D. Awschalom, PNAS **107**, 8513 (2010).

[24] A. Gali, Phys. Status Solidi B **248**, 1337 (2011).

[25] W. F. Koehl, B. B. Buckley, F. J. Heremans, G. Calusine, and D. D. Awschalom, Nature **479**, 84 (2011).

[26] A. L. Falk, P. V. Klimov, B. B. Buckley, V. Ivády, I. A. Abrikosov, G. Calusine, W. F. Koehl, A. Gali, and D. D. Awschalom, Phys. Rev. Lett. **112**, 187601 (2014).

[27] P. Udvarhelyi and A. Gali, Phys. Rev. Appl. **10**, 054010 (2018).

[28] S. J. Whiteley, G. Wolfowicz, C. P. Anderson, A. Bourassa, H. Ma, M. Ye, G. Koolstra, K. J. Satzinger, M. V. Holt, F. J. Heremans, A. N. Cleland, D. I. Schuster, G. Galli, and D. D. Awschalom, Nat. Phys. **15**, 490 (2019).

[29] D. Riedel, F. Fuchs, H. Kraus, S. Väth, A. Sperlich, V. Dyakonov, A. A. Soltamova, P. G. Baranov, V. A. Ilyin, and G. V. Astakhov, Phys. Rev. Lett. **109**, 226402 (2012).

[30] D. Simin, V. A. Soltamov, A. V. Poshakinskiy, A. N. Anisimov, R. A. Babunts, D. O. Tolmachev, E. N. Mokhov, M. Trupke, S. A. Tarasenko, A. Sperlich, P. G. Baranov, V. Dyakonov, and G. V. Astakhov, Phys. Rev. X **6**, 031014 (2016).

[31] C. J. Cochrane, J. Blacksberg, M. A. Anders, and P. M. Lenahan, Sci. Rep. **6**, srep37077 (2016).

[32] A. N. Anisimov, D. Simin, V. A. Soltamov, S. P. Lebedev, P. G. Baranov, G. V. Astakhov, and V. Dyakonov, Sci. Rep. **6**, 33301 (2016).

[33] M. Niethammer, M. Widmann, T. Rendler, N. Morioka, Y.-C. Chen, R. Stöhr, J. Ul Hassan, S. Onoda, T. Ohshima, S.-Y. Lee, A. Mukherjee, J. Isoya, N. T. Son, and J. Wrachtrup, Nat. Commun. **10**, 5569 (2019).

[34] G. Wolfowicz, C. P. Anderson, A. L. Yeats, S. J. Whiteley, J. Niklas, O. G. Poluektov, F. J. Heremans, and D. D. Awschalom, Nat. Commun. **8**, 1876 (2017).

[35] D. A. Golter and C. W. Lai, Sci. Rep. **7**, 13406 (2017).

[36] B. Magnusson, N. T. Son, A. Csóré, A. Gällström, T. Ohshima, A. Gali, and I. G. Ivanov, Phys. Rev. B **98**, 195202 (2018).

[37] W. Klahold, C. Tabachnick, G. Freedman, R. P. Devaty, and W. J. Choyke, in *Silicon Carbide and Related Materials 2016*, Materials Science Forum, Vol. 897 (Trans Tech Publications, Switzerland, 2017), pp. 250–253.

[38] P. Käckell, B. Wenzien, and F. Bechstedt, Phys. Rev. B **50**, 10761 (1994).

[39] W. R. L. Lambrecht, S. Limpijumnong, S. N. Rashkeev, and B. Segall, Phys. Status Solidi B **202**, 5 (2001).

[40] See Supplemental Material at http://link.aps.org/supplemental/10.1103/PhysRevMaterials.4.014601 for band structure, quasiparticle correction, convergence tests on electron-phonon coupling, phonons, and carrier conductivity.

[41] P. Giannozzi, O. Andreussi, T. Brumme, O. Bunau, M. B. Nardelli, M. Calandra, R. Car, C. Cavazzoni, D. Ceresoli, M. Cococcioni, N. Colonna, I. Carnimeo, A. D. Corso, S. de Gironcoli, P. Delugas, R. A. D. Jr, A. Ferretti, A. Floris, G. Fratesi, G. Fugallo, R. Gebauer, U. Gerstmann, F. Giustino, T. Gorni, J. Jia, M. Kawamura, H.-Y. Ko, A. Kokalj, E. Küçükbenli, M. Lazzeri, M. Marsili, N. Marzari, F. Mauri, N. L. Nguyen, H.-V. Nguyen, A. O. de-la Roza, L. Paulatto, S. Poncé, D. Rocca, R. Sabatini, B. Santra, M. Schlipf, A. P. Seitsonen, A. Smogunov, I. Timrov, T. Thonhauser, P. Umari, N. Vast, X. Wu, and S. Baroni, J. Phys.: Condens. Matter **29**, 465901 (2017).

[42] J. P. Perdew and A. Zunger, Phys. Rev. B **23**, 5048 (1981).

[43] M. Stockmeier, R. Müller, S. A. Sakwe, P. J. Wellmann, and A. Magerl, J. Appl. Phys. **105**, 033511 (2009).

[44] L. Patrick, Phys. Rev. **167**, 809 (1968).

[45] D. W. Feldman, J. H. Parker, W. J. Choyke, and L. Patrick, Phys. Rev. **173**, 787 (1968).

[46] D. W. Feldman, J. H. Parker, W. J. Choyke, and L. Patrick, Phys. Rev. **170**, 698 (1968).

[47] H. Nienhaus, T. Kampen, and W. Mönch, Surf. Sci. **324**, L328 (1995).

[48] S. Nakashima and H. Harima, Phys. Status Solidi A **162**, 39 (1997).

[49] J. Bluet, K. Chourou, M. Anikin, and R. Madar, Mater. Sci. Eng. B **61-62**, 212 (1999).

[50] S. Poncé, G. Antonius, Y. Gillet, P. Boulanger, J. Laflamme Janssen, A. Marini, M. Côté, and X. Gonze, Phys. Rev. B **90**, 214304 (2014).

[51] A. Marini, S. Poncé, and X. Gonze, Phys. Rev. B **91**, 224310 (2015).

[52] P. B. Allen and V. Heine, J. Phys. C: Solid State Phys. **9**, 2305 (1976).

[53] P. B. Allen and M. Cardona, Phys. Rev. B **23**, 1495 (1981).

[54] P. B. Allen and M. Cardona, Phys. Rev. B **27**, 4760 (1983).

[55] D. Sangalli, A. Ferretti, H. Miranda, C. Attaccalite, I. Marri, E. Cannuccia, P. Melo, M. Marsili, F. Paleari, A. Marrazzo, G. Prandini, P. Bonfà, M. O. Atambo, F. Affinito, M. Palummo, A. Molina-Sánchez, C. Hogan, M. Grüning, D. Varsano, and A. Marini, J. Phys.: Condens. Matter **31**, 325902 (2019).

[56] S. Baroni, S. de Gironcoli, A. Dal Corso, and P. Giannozzi, Rev. Mod. Phys. **73**, 515 (2001).

[57] *Semiconductors Physics of Group IV Elements and III-V Compounds*, edited by K. Hellwege, O. Madelung, and Landolt-Börnstein, Vol. 12: Magnetic and Other Properties of Oxides and Related Compounds, Part c: Hexagonal Ferrites. Special Lanthanide and Actinide Compounds (Springer, Berlin, 1982).

[58] R. T. M. Ummels, P. A. Bobbert, and W. van Haeringen, Phys. Rev. B **58**, 6795 (1998).

[59] M. Nakabayashi, T. Fujimoto, M. Katsuno, and N. Ohtani, in *Silicon Carbide and Related Materials 2005*, Materials Science Forum, Vol. 527 (Trans Tech Publications, Switzerland, 2006), pp. 699–702.

[60] B. Monserrat and R. J. Needs, Phys. Rev. B **89**, 214304 (2014).
[61] P. Ščajev and K. Jarašiūnas, J. Phys. D **42**, 055413 (2009).
[62] R. W. Godby and R. J. Needs, Phys. Rev. Lett. **62**, 1169 (1989).
[63] L. Hedin, Phys. Rev. **139**, A796 (1965).
[64] L. Hedin and S. Lindqvist, Solid State Phys. **23**, 1 (1969).
[65] M. Bockstedte, A. Marini, O. Pankratov, and A. Rubio, Phys. Rev. Lett. **105**, 026401 (2010).
[66] G. E. Engel and B. Farid, Phys. Rev. B **47**, 15931 (1993).
[67] C. Friedrich, M. C. Müller, and S. Blügel, Phys. Rev. B **84**, 039906(E) (2011).
[68] M. Stankovski, G. Antonius, D. Waroquiers, A. Miglio, H. Dixit, K. Sankaran, M. Giantomassi, X. Gonze, M. Côté, and G.-M. Rignanese, Phys. Rev. B **84**, 241201(R) (2011).
[69] C. H. Park, B.-H. Cheong, K.-H. Lee, and K. J. Chang, Phys. Rev. B **49**, 4485 (1994).
[70] B. Wenzien, P. Käckell, F. Bechstedt, and G. Cappellini, Phys. Rev. B **52**, 10897 (1995).
[71] V. I. Sankin, Fiz. Tverd. Tela (Leningrad) **17**, 1820 (1975) [Sov. Phys. Solid State **17**, 1191 (1975)].
[72] G. B. Dubrovskii and V. I. Sankin, Fiz. Tverd. Tela (Leningrad) **17**, 1847 (1975) [Sov. Phys. Solid State **17**, 1847 (1975)].
[73] Y.-i. Matsushita, S. Furuya, and A. Oshiyama, Phys. Rev. Lett. **108**, 246404 (2012).
[74] N. T. Son, W. M. Chen, O. Kordina, A. O. Konstantinov, B. Monemar, E. Janzén, D. M. Hofman, D. Volm, M. Drechsler, and B. K. Meyer, Appl. Phys. Lett. **66**, 1074 (1995).
[75] G. Grosso and G. Pastori Parravicini, *Solid State Physics* (Academic Press, US, 2000).
[76] G. Yepifanov, *Physical Principles of Micro-Electronics* (MIR Publichers Moscow, Moscow, Russia, 1974).
[77] T. Takase, M. Sakaino, Y. Sun, and T. Miyasato, Jpn. J. Appl. Phys. **52**, 091301 (2013).
[78] A. Beste, DeCarlos E. Taylor, D. A. Golter, and C. W. Lai, Phys. Rev. B **98**, 214107 (2018).
[79] F.-F. Yan, J.-F. Wang, Q. Li, Z.-D. Cheng, J.-M. Cui, W.-Z. Liu, J.-S. Xu, C.-F. Li, and G.-C. Guo, Phys. Rev. Appl. **10**, 044042 (2018).